

14 Beam Envelope Techniques for Ion-Optical Calculations

S. Bazhal¹ and R. Hellborg²

¹ SSC RF Institute for Physics and Power Engineering, 1 Bondarenko Sq.,
Obninsk, Kaluga Region, 249033 Russia
bazhal@ippe.obninsk.ru

² Department of Physics, Lund University, Sölvegatan 14, 223 62 Lund, Sweden
ragnar.hellborg@nuclear.lu.se

14.1 Introduction

The understanding of the analogy between propagation of light rays in a nonuniform medium and the motion of electrons in an electromagnetic field, outlined in the 1930s, served as a stimulus for the development of charged-particle optics. In the initial stage of its development, charged-particle optics mainly considered the problem of image acquisition by means of electrons. In a short time, this area of study named “electron optics” resulted in the development of the electron microscope. However, the problems of electron optics were not confined to development of a lens system for providing images with the help of electron beams. The expanding applications of electron and ion beams required the development of devices capable of providing the necessary control of beams and to deliver charged particles from their source to a distant target. The appearance and rapid growth of ion optics, for example, were mainly caused by the need for mass analysis, as well as by the development of charged-particle accelerators. To date, charged-particle optics embraces a wide range of problems connected with the application of electron and ion beams in different areas of science and technology. A huge number of publications have been devoted to this subject. Unfortunately, it is impossible to give even a brief overview of these publications in the framework of this chapter. Therefore we confine ourselves to references to the books [1–3], in which the principles of charged-particle optics are given along with an extensive bibliography.

One of the fields of application of ion optics is electrostatic accelerators. Ion-optical calculations play there (as in all other applications) a large role. The techniques for ion-optical calculations for electrostatic accelerators have undergone a very thorough change during their history of more than half a century (one of the first papers in which a detailed calculational analysis of an ion-optical system of an electrostatic accelerator was given was published in 1953 [4]). These techniques have come a long way from simple analytical calculations based on approximations of geometrical optics, towards sophisticated 3-D computer simulation. The rapid development of hardware will probably promote the creation of increasingly complicated software for

mathematical simulation of ion-optical systems. However, as was mentioned by J.D. Larson [5], application of complex numerical models without preliminary analytical calculations is fraught with the risk that the understanding of the results obtained could be lost. This observation, in spite of the impressive development of a system for data visualization, seems to remain valid in the future as well. Therefore it is essential to begin the solution of any ion-optical problems with simple analytical evaluations, then passing on to numerical calculations based on simplified mathematical models, and to use more complicated calculation techniques only at the last stage if necessary.

Electrostatic accelerators are widely used in various fields of scientific research and in industry. Quite naturally, the range of ion-optical problems arising at these accelerators is wide enough, and rather different approaches are necessary for their solution. Suffice it to mention ion microprobes and bunched beams as examples of the variety of these problems. At the same time, there is a problem that is general for the majority of applications. This is the beam transport problem.

Some examples of uncomplicated ion-optical calculations (both analytical and numerical) which can be used for electrostatic accelerators will be given in this chapter. The main attention is paid to methods for first-order calculations of beam transport taking into account the unordered spread of transverse speeds of ions, as well as the space charge forces. To describe a continuous monoenergetic ion beam, we use the concepts of four-dimensional phase space and of beam envelopes. According to Liouville's theorem, the phase volume occupied by the points representing the ion beam in the 4-D space of canonically conjugate coordinates and momenta is conserved. In the case of separation of variables in the equations of motion, projections of the phase volume on the planes of canonically conjugate variables are conserved as well. More often, however, to describe the transverse motion of ions, one considers the projection of the phase volume onto a plane of coordinates and angles, the plane XX' for example. The area of this projection divided by π , called the emittance ϵ , is an important characteristic of a charged-particle beam:

$$\epsilon = \frac{1}{\pi} \int \int dx dx' \quad (14.1)$$

It is known that for a beam with finite (i.e. nonzero) emittance, one cannot point out a particle the trajectory of which could define a beam boundary. In this case the boundary is defined by an envelope of the ion trajectories, the determination of which is one of the principal problems for beams with finite emittance. To find the beam envelope in a linear approach one generally uses the matrix formalism or the solution of differential equations for the envelope. Detailed descriptions of these methods can be found in [6–9].

14.2 An Analytical Technique for Calculation of Ion Beam Envelopes

Let us consider some simple calculation techniques which can be useful in the first stage of designing the ion-optical system of an electrostatic accelerator, as well as for analysis of the optical behavior of elements of this system. The method we shall use was suggested by E.V. Shpak [10]. For an ion beam with a negligibly small current, this method allows one to find an analytical expression for the beam envelope from a family of trajectories passing through a boundary of the projection of the 4-D phase volume. In the original method [10], an analytical expression for the beam envelope is found as a function of the longitudinal coordinate z on the assumption that the beam has a crossover at the initial point z_0 (i.e. the beam in the phase plane is represented at this point by a straight ellipse).

We consider the method in more detail, having generalized it to initial conditions given by an elliptical phase contour with an arbitrarily sloped axis. We assume that at the initial point z_0 , the projection of the phase volume of the beam onto the plane XX' is bounded by an ellipse given by

$$\gamma x_0^2 + 2\alpha x_0 x'_0 + \beta (x'_0)^2 = \epsilon \quad (14.2)$$

The relations between the coefficients α , β and γ in (14.2) and the input characteristics of the beam (the envelope coordinate r_0 , the beam divergence r'_0 and the emittance ϵ) are given by the following:

$$\begin{aligned} \alpha &= -\frac{r_0 r'_0}{\epsilon} \\ \beta &= \frac{r_0^2}{\epsilon} \\ \gamma &= \frac{\epsilon^2 + (r_0 r'_0)^2}{\epsilon r_0^2} \end{aligned} \quad (14.3)$$

Let the projection of the ion trajectory on the coordinate plane XOZ be given by

$$x(z) = R_1(z)x_0 + R_2(z)x'_0 \quad (14.4)$$

where $R_1(z)$ and $R_2(z)$ are linearly independent solutions of the paraxial equation ($R_1(0) = 1$; $R'_1(0) = 0$; $R_2(0) = 0$; $R'_2(0) = 1$); and x_0 and x'_0 are the initial values of the transverse coordinate of the ion and the tangent of the angle between the ion trajectory and the longitudinal axis OZ , respectively. Equation (14.5), obtained from (14.2)–(14.4), gives a family of ion trajectories

$$x(z) - R_1(z)x_0 - R_2(z) \left(\frac{r'_0}{r_0} x_0 \pm \frac{\epsilon}{r_0} \sqrt{r_0^2 - x_0^2} \right) = 0 \quad (14.5)$$

The initial points of the trajectories (14.5) are located on the boundary phase contour given by (14.2). The beam envelope can be determined as the envelope of the family of the curves given by (14.5). After elimination of x_0 from

the simultaneous equations

$$\begin{aligned} F(x_0, z) &= 0 \\ \frac{\partial F(x_0, z)}{\partial x_0} &= 0 \end{aligned} \quad (14.6)$$

where $F(x_0, z)$ denotes the left-hand side of (14.5), we arrive at an expression for the calculation of the envelope,

$$r(z) = \pm \sqrt{(R_1(z)r_0 + R_2(z)r'_0)^2 + \left(\frac{R_2(z)\epsilon}{r_0}\right)^2} \quad (14.7)$$

Note that (14.7) agrees with a particular solution of the differential equation for the beam envelope given in [7]. Finding the derivative of r with respect to z , we arrive at an expression for the beam divergence r' :

$$r'(z) = \pm \frac{(R_1 r_0 + R_2 r'_0)(R'_1 r_0 + R'_2 r'_0) + R_2 R'_2 (\epsilon/r_0)^2}{r(z)} \quad (14.8)$$

(The signs “+” and “−” in (14.7) and (14.8) are related to the upper and lower branches of the envelope, respectively) And finally, equating the right-hand side of (14.8) to zero, one can find a position of the beam crossover.

We shall now consider two examples of the application of the analytical expression (14.7) to beam envelope calculation for elements of the ion-optical system of an electrostatic accelerator.

14.2.1 Focusing of an Ion Beam with Finite Emittance by an Accelerator Tube

Let us turn to Elkind’s classic work [4], in which a detailed analysis of beam focusing by an accelerator tube was given for the first time. The calculations represented in Elkind’s work were performed in the approach of geometrical optics (i.e. for a beam with zero emittance). Therefore they did not take into account the effect of an unordered spread of ion speeds on the beam focusing. We shall now solve Elkind’s problem for a beam with finite emittance.

Let the system for beam acceleration and transport consist of the following linear optical elements (Fig. 14.1): 1, a drift section between the plane of optical object and the accelerator tube; 2, a converging aperture lens at the entrance to the accelerator tube; 3, an uniform-field accelerator tube; 4 a diverging aperture lens at the exit of the accelerator tube; and 5, a drift section between the accelerator tube and the target on which the beam has to be focused [4]. The problem will be solved without taking into consideration the space charge forces. In this case the variables in the equations of motion are separated. Therefore the analysis can be confined to one of the coordinate planes (XOZ , for example).

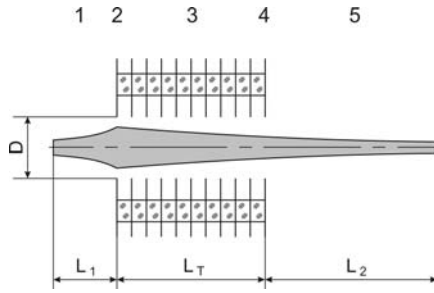


Fig. 14.1. For calculation of beam-focusing by an accelerator tube

Consider the motion of nonrelativistic ions in the drift section following the accelerator tube (Fig. 14.1, part 5). In this section the projection of the trajectory on the coordinate plane takes the form of (14.4). Using matrix formalism, we now determine $R_1(z)$ and $R_2(z)$ in (14.4). The transfer matrix of the whole system (parts 1–5 in Fig. 14.1),

$$\mathbf{R}_S = \begin{pmatrix} R_{11} & R_{12} \\ R_{21} & R_{22} \end{pmatrix} \tag{14.9}$$

can be expressed as a matrix product of its individual ion-optical elements:

$$\mathbf{R}_S = \mathbf{R}_2 \mathbf{R}_D \mathbf{R}_T \mathbf{R}_F \mathbf{R}_1 \tag{14.10}$$

where

$$\mathbf{R}_1 = \begin{pmatrix} 1 & L_1 \\ 0 & 1 \end{pmatrix} \tag{14.11}$$

is the matrix of the drift section located before the accelerator tube (Fig. 14.1, part 1);

$$\mathbf{R}_F = \begin{pmatrix} 1 & 0 \\ 1/f_1 & 1 \end{pmatrix} \tag{14.12}$$

is the matrix of the input aperture lens (Fig. 14.1, part 2);

$$\mathbf{R}_T = \begin{pmatrix} 1 & 2L_T/(\sqrt{N} + 1) \\ 0 & 1/\sqrt{N} \end{pmatrix} \tag{14.13}$$

is the matrix of the uniform-field accelerator tube (Fig. 14.1, part 3);

$$\mathbf{R}_D = \begin{pmatrix} 1 & 0 \\ 1/f_2 & 1 \end{pmatrix} \tag{14.14}$$

is the matrix of the output aperture lens (Fig. 14.1, part 4); and, finally,

$$\mathbf{R}_2 = \begin{pmatrix} 1 & L_2 \\ 0 & 1 \end{pmatrix} \tag{14.15}$$

is the matrix of the drift section positioned after the accelerator tube (Fig. 14.1, part 5).

The following notation is used for the matrix elements: $N = \Phi_l/\Phi_0$ is the ratio of the potential of the last electrode of the accelerator tube to the potential of the first tube electrode; f_1 and f_2 are the focal lengths of the input and output aperture lenses; and L_1 , L_T and L_2 are the lengths of the first drift section, of the accelerator tube and of the second drift section, respectively (see Fig. 14.1).

The focal length of the aperture lens can be approximated by $f = 4\Phi\xi/(E_1 - E_2)$, where ξ is a function of $\Phi/(E_1 - E_2)$ and the aperture diameter D [4], and E_1 and E_2 are the fields preceding and following the aperture, respectively. For the weak output lens, this dependence can be neglected, assuming $\xi = 1$. Then, using the ratio N defined above, we arrive at

$$f_1 = -4\xi L_T/(N - 1) \quad (14.16)$$

$$f_2 = 4NL_T/(N - 1) \quad (14.17)$$

Taking into consideration (14.10)–(14.17), one can write the matrix elements R_{11} and R_{12} as

$$R_{11} = \frac{3(N - 1)(\xi - \sqrt{N})L_2}{8N\xi L_T} - \frac{\sqrt{N} - 1}{2\xi} + 1 \quad (14.18)$$

$$R_{12} = \frac{L_2}{2N} \left\{ \frac{L_1(N - 1)}{2L_T} + (3\sqrt{N} - 1) \left[1 - \frac{L_1(N - 1)}{4\xi L_T} \right] \right\} + \frac{2L_T(\sqrt{N} - 1)}{N - 1} \left[1 - \frac{L_1(N - 1)}{4\xi L_T} \right] + L_1 \quad (14.19)$$

We suppose now that the beam is focused into a waist with a radius of r_0 at a distance of L_1 from the entrance aperture lens. Let us find the distance L_2 from the exit aperture at which the output crossover is shaped. Assuming the plane of this crossover to be the end of the ion-optical system under consideration, one can write $R_1(z) = R_{11}$ and $R_2(z) = R_{12}$. Having substituted (14.18) and (14.19) into (14.7), we differentiate it with respect to z , taking into account the obvious relation between variables z and L_2 : $z = L_1 + L_T + L_2$. Solving the equation obtained in such a way with respect to L_2 , we determine the position of the output crossover

$$L_2 = \frac{4NL_T(\sqrt{N} - 1 - 2\xi)(r_0^4 + \epsilon^2 S_1 S_2)}{3(N - 1)(\xi - \sqrt{N})(r_0^4 + \epsilon^2 S_2^2)} \quad (14.20)$$

where $S_1 = 4L_T\xi/((\sqrt{N} + 1)(\sqrt{N} - 1 - 2\xi)) - L_1$ and $S_2 = 4L_T\xi(3\sqrt{N} - 1)/(3(N - 1)(\sqrt{N} - \xi)) - L_1(3\sqrt{N} - 1 - 2\xi)/(3(\sqrt{N} - \xi))$. In the extreme case of a beam of zero emittance, emerging from a point source on the optical axis (i.e. for $\epsilon \rightarrow 0$ and $r_0 \rightarrow 0$), (14.20) transforms to Elkind's formula:

$$L_2 = 4NL_T \frac{(\sqrt{N} - 1 - 2\xi) - 4\xi(L_T/L_1)/(\sqrt{N} + 1)}{4\xi(L_T/L_1)(3\sqrt{N} - 1) - (N - 1)(3\sqrt{N} - 1 - 2\xi)} \quad (14.21)$$

As a rule, $N \gg 1$ for electrostatic accelerators. Then a condition for existence of a beam crossover in the drift space following the accelerator tube is given by the inequality $S_1 S_2 < -r_0^4/\epsilon_0^2$. This inequality defines more rigid constraints for the position of the input crossover in comparison with the analogous inequality $S_1 S_2 < 0$ obtained from Elkind's formula (14.21).

One of the ion-optical problems for electrostatic accelerators lies in matching the beam to the accelerator tube. By defining a relation between the positions of the input and output crossovers, (14.20) allows us to perform estimations necessary for this problem to be solved. These estimations will be done using the low-energy accelerator tube of the 3 MV Pelletron tandem accelerator in Lund as an example. The beam-matching problem at this accelerator has already been solved earlier by a matrix method [11]. By analogy with this work, we employ in our example a simplified approximation for the input aperture lens, assuming ξ in (14.20) to be equal to unity. We shall also assume that the electrostatic field in the accelerator tube ($L_T = 1.694$ m) is uniform. Figure 14.2 gives the relationship $L_2 = f(L_1)$ calculated for the fixed ratio $N = 60$. Here the variable parameters are the radius r_0 of the beam in the plane of the input crossover and the normalized emittance ϵ_n (Fig. 14.2, curves 1–4). Curve 5, giving the relationship between the positions

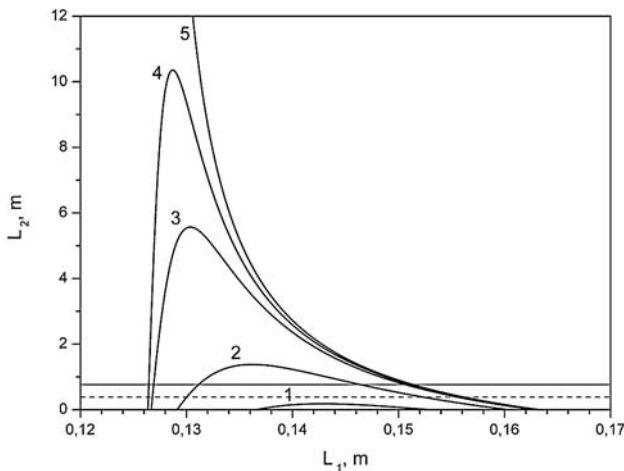


Fig. 14.2. Relationships between the positions of the input (L_1) and output (L_2) crossovers calculated for the low-energy part of the accelerator tube of the 3 MV Pelletron accelerator in Lund. 1, $\epsilon_n = 3\pi \times 10^{-6}$ m rad (MeV) $^{0.5}$, $r_0 = 0.5 \times 10^{-3}$ m; 2, $\epsilon_n = 5\pi \times 10^{-6}$ m rad (MeV) $^{0.5}$, $r_0 = 0.5 \times 10^{-3}$ m; 3, $\epsilon_n = 3\pi \times 10^{-6}$ m rad (MeV) $^{0.5}$, $r_0 = 0.25 \times 10^{-3}$ m; 4, $\epsilon_n = 5\pi \times 10^{-6}$ m rad (MeV) $^{0.5}$, $r_0 = 0.25 \times 10^{-3}$ m; 5, $\epsilon_n = 0$, $r_0 = 0$ (the calculation performed in accordance with Elkind's approximation)

of an optical object located in the drift space before the accelerator tube and its image created by the tube was calculated in Elkind's approach (14.21). For the purpose of more detailed analysis, the drift space after the accelerator tube has not been constrained to the actual drift section under the high-voltage terminal of the Pelletron accelerator (the boundary of this drift section is shown in Fig. 14.2 as a solid horizontal line). Consider the focusing of the beam onto the center of the stripper (the center of the stripper channel is marked by a dashed line). As can be seen from Fig. 14.2, the functional dependences $L_2 = f(L_1)$ plotted for a beam with finite emittance (curves 1–4 in Fig. 14.2) have a maximum. This highest possible value of L_2 decreases with increasing beam radius r_0 in the plane of the input crossover and with decreasing emittance ϵ_n . The curve 1 is completely below the dashed line, i.e. in this case the crossover cannot be obtained at the center of the stripper. The dashed line, as can be seen in Fig. 14.2, crosses the curves 2–4 twice, giving two values of L_1 for which the output crossover is in the center of the stripper. However, the lower of these two values of L_1 corresponds to an impermissible large optical magnification and therefore cannot be applied in practice. To obtain a beam crossover at the stripper, the beam needs to have a rather small radius in the plane of the input crossover and, in addition, the permissible position for this plane is constrained to quite a small part of the input drift section. The calculation and experimental results given in [11] justify this conclusion. Thus the ion-optical behavior of the system under consideration imposes a rigid limitation upon the input characteristics of the beam.

14.2.2 Application of the Beam Envelope Technique for Acceptance Calculations

Let us consider an application of the beam envelope technique to calculation of the acceptance of a part of an ion-optical system confined between two apertures. Although this problem had been already discussed by J.D. Larson and C.M. Jones in detail [12], we decided to return to the problem for the following reasons. Firstly, in the case of an elliptical phase contour, the envelope technique allows somewhat of a simplification of the derivation of the main formula for the acceptance calculation. Secondly, the method suggested gives a possibility of graphical representation of the results in the phase plane.

Then let a part of some ion-optical channel be confined between two planes z_0, z_1 . Let r_0, r_1 be, correspondingly, the radii of the input and the output apertures constraining the beam in these planes. For this part of the system, we shall derive an analytical expression for the acceptance making use of (14.7). If $R_2(z_1) = 0$, i.e. the system under consideration forms a Gaussian image in the plane z_1 , then (14.7) takes the form $r_1 = |R_1(z_1)|r_0$. In this case the transverse dimension of the beam in the image plane does not depend on the beam emittance, and it is determined by the absolute value of the

optical magnification of the system. Assuming $R_2(z_1) \neq 0$, we can express the emittance ϵ from (14.7) as

$$\epsilon = \sqrt{\left(\frac{r_0 r_1}{R_2(z_1)}\right)^2 - \left(\frac{r_0[R_1(z_1)r_0 + R_2(z_1)r'_0]}{R_2(z_1)}\right)^2} \quad (14.22)$$

Equations (14.2), (14.3) and (14.22) determine in the phase plane a family of ellipses of variable area $\pi\epsilon$. The ellipses exist under conditions given by the inequality $r_1^2 - (R_1 r_0 + R_2 r'_0)^2 > 0$. Its solution establishes the variation limits for the beam divergence r'_0 :

$$\begin{aligned} -(R_1/R_2)r_0 - (|r_1|/R_2) < r'_0 < -(R_1/R_2)r_0 + (|r_1|/R_2); R_2 > 0 \\ -(R_1/R_2)r_0 + (|r_1|/R_2) < r'_0 < -(R_1/R_2)r_0 - (|r_1|/R_2); R_2 < 0. \end{aligned} \quad (14.23)$$

The emittance reaches its maximum value when the second term under the square root in (14.22) is equal to zero, i.e.

$$r'_0 = -\frac{R_1}{R_2}r_0 \quad (14.24)$$

The upper bound of the emittance determines the acceptance A ; it follows directly that

$$A = \left| \frac{r_0 r_1}{R_2} \right| \quad (14.25)$$

Taking into account that the emittance has been defined in the present work as the area of a phase ellipse divided by π , (14.25) coincides with the expression derived in [12]. Substituting (14.24) and (14.25) in the coefficients of (14.3), we arrive at the equation representing the acceptance in the phase plane:

$$\left(\frac{r_1^2 + r_0^2 R_1^2}{r_0^2 r_1^2}\right) x^2 + \frac{2R_1 R_2}{r_1^2} x x' + \frac{R_2^2}{r_1^2} (x')^2 = 1 \quad (14.26)$$

As an example we present acceptance calculations performed for the mass analyzer of the injector at the Pelletron accelerator in Lund [13]. The mass analyzer is a uniform-field dipole magnet with a bending angle $\varphi = 90^\circ$, a bending radius $\rho_m = 0.3735$ m and an angle of pole edge rotation $\beta = 28.2^\circ$. The cross section of the vacuum chamber of the mass analyzer has the following dimensions: 80 mm in the dispersive plane and 39 mm in the non-dispersive plane. The planes of the optical object and image are at equal distances from the boundaries of the magnetic field. A four-blade input aperture is positioned in the object plane of the magnetic analyzer. A two-blade slit device is installed in the image plane.

Since the trajectory R_2 crosses the optical axis in the image plane (i.e. $R_2 = 0$ in this plane), the analyzer acceptance does not depend on the aperture of the slit device. It is defined only by the input aperture which is used as the first diaphragm in (14.25) and by the aperture of the vacuum chamber

of the analyzer. For a wide range of initial beam conditions (beam radius, divergence and emittance), the beam envelope reaches a maximum inside the analyzer. Therefore, to use the transverse dimensions of the vacuum chamber of the analyzer in acceptance calculations performed by the “two diaphragm” formula (14.25), we have to find a cross section of the vacuum chamber that represents the chamber constraints equivalently and hence could be considered as the second diaphragm.

Consider first the dispersive (XOZ) plane of the magnetic analyzer. In this plane, the beam is defocused by the fringe fields and focused by the uniform magnetic field. Focusing is the resulting effect. Therefore, it is most natural to connect the position of the second diaphragm with a possible maximum of the beam envelope in the uniform-field region. Then, using (14.8), we can find this maximum from the equation

$$(R_1 r_0 + R_2 r'_0)(R'_1 r_0 + R'_2 r'_0) + \left(\frac{\epsilon}{r_0}\right)^2 R_2 R'_2 = 0 \tag{14.27}$$

Taking into account that $R_1 r_0 + R_2 r'_0 = 0$ for the beam of the maximum possible emittance, and that the image plane is outside the magnetic field (i.e. $R_2 \neq 0$ in the field region), we arrive at the condition for the extreme of the R_2 trajectory,

$$R'_2 = 0 \tag{14.28}$$

Thus, the position of the second diaphragm coincides with the extreme of the trajectory $R_2(z)$ determined by a linearly independent solution of the paraxial equation.

To find the trajectory $R_2(z)$ in the field region of the magnetic analyzer, we use the matrix formalism. The transfer matrix of the system, consisting of a drift section between the input aperture and the effective boundary of the magnetic field, a thin lens describing the effect of the fringe field, and the sector magnetic field can be expressed as a matrix product of these individual elements:

$$\mathbf{R} = \mathbf{R}_M \mathbf{R}_L \mathbf{R}_{Dr} \tag{14.29}$$

where

$$\mathbf{R}_M = \begin{pmatrix} \cos(z/\rho_m) & \rho_m \sin(z/\rho_m) \\ -\rho_m^{-1} \sin(z/\rho_m) & \cos(z/\rho_m) \end{pmatrix} \tag{14.30}$$

$$\mathbf{R}_L = \begin{pmatrix} 1 & 0 \\ \rho_m^{-1} \tan \beta & 1 \end{pmatrix} \tag{14.31}$$

$$\mathbf{R}_{Dr} = \begin{pmatrix} 1 & L \\ 0 & 1 \end{pmatrix} \tag{14.32}$$

are the matrices of the uniform magnetic field, of the fringing-field lens and of the drift section of length L , respectively. Multiplication of the matrices yields

$$R_2(\theta) = L \cos \theta + (L \tan \beta + \rho_m) \sin \theta \quad (14.33)$$

where $\theta = z/\rho_m$. The trajectory $R_2(\theta)$ attains an extreme at

$$\theta_e = \arctan \left(\tan \beta + \frac{\rho_m}{L} \right), \quad |\theta| \leq 90^\circ \quad (14.34)$$

After substituting θ_e in (14.33), we find this extreme of the trajectory R_2 :

$$R_2(\theta_e) = L \sqrt{1 + \left(\tan \beta + \frac{\rho_m}{L} \right)^2} \quad (14.35)$$

In the field region of the 90° magnet, the extreme is a maximum for any L , since $R_2 > 0$ and $R_2'' = -R_2$ at the point of the extreme. Taking into consideration the condition for radial focusing in a uniform sector magnetic field [3],

$$\sin \varphi + 2 \frac{L \cos(\varphi - \beta)}{\rho_m \cos \beta} - \left(\frac{L}{\rho_m \cos \beta} \right)^2 \sin(\varphi - 2\beta) = 0 \quad (14.36)$$

as well as equality of the distances from the field boundaries to the object and image planes, one can express L through the geometrical parameters of the analyzer:

$$L = \frac{\rho_m}{1 - \tan \beta} \quad (14.37)$$

And finally, substituting (14.37) in to (14.35), we arrive at an expression for the extreme of the trajectory R_2 :

$$R_2 = \frac{\rho_m \sqrt{2}}{1 - \tan \beta} \quad (14.38)$$

R_1 can also be expressed through the matrix product given by (14.29). Substituting the value of θ_e in this expression at the point of the extreme of the trajectory R_2 yields

$$R_1 = \frac{1 + \tan \beta}{\sqrt{2}} \quad (14.39)$$

Equations (14.38) and (14.39) and the dimensions of the two diaphragms determine an acceptance area in the phase plane. In accordance with (14.25), the value of the acceptance in the dispersive plane of the magnetic analyzer can be calculated from:

$$A = \frac{r_{x0} r_{x1} (1 - \tan \beta)}{\rho_m \sqrt{2}} \quad (14.40)$$

where $2r_{x0}$ and $2r_{x1}$ define the input aperture and the aperture of the vacuum chamber of the magnetic analyzer, respectively.

In the nondispersive (YOZ) plane of the magnetic analyzer, only the fringe field lenses act as focusing elements. In the first-order approach, the

absolute value of the focal length of the lenses is the same for both of the transverse planes. Therefore the transfer matrices \mathbf{R}_M and \mathbf{R}_L can be written as

$$\mathbf{R}_M = \begin{pmatrix} 1 & z \\ 0 & 1 \end{pmatrix} \tag{14.41}$$

$$\mathbf{R}_L = \begin{pmatrix} 1 & 0 \\ -\rho_m^{-1} \tan \beta & 1 \end{pmatrix} \tag{14.42}$$

Substitution of (14.41) and (14.42) in (14.29) yields

$$R_1 = 1 - \frac{z \tan \beta}{\rho_m} \tag{14.43}$$

$$R_2 = \frac{\rho_m}{1 - \tan \beta} + z \frac{1 - 2 \tan \beta}{1 - \tan \beta} \tag{14.44}$$

In the magnetic-field region, the trajectory R_2 neither attains the extremes nor crosses the optical axes. Taking into account that $1 - 2 \tan \beta < 0$ in (14.44), we arrive at the expressions for the acceptance calculation

$$R_1 = 1 ; \quad R_2 = \frac{\rho_m}{1 - \tan \beta} ; \quad A = \frac{r_{y0} r_{y1} (1 - \tan \beta)}{\rho_m} \tag{14.45}$$

Finally, let us consider a numerical example. Let the opening of the four-blade input aperture be $5 \times 5 \text{ mm}^2$. To reduce the unfavorable effect of aberration, we require that the beam dimensions in two transverse planes do not exceed half of the aperture of the vacuum chamber of the analyzer. This requirement results, evidently, in smaller acceptances in comparison with those which are defined by the geometrical constraints of the chamber. Taking into consideration that $2r_{x1} = 40 \text{ mm}$ and $2r_{y1} = 19.5 \text{ mm}$, we obtain the following values of these “conditional” acceptances: $A_x = 44 \text{ mm mrad}$ for the dispersive plane and $A_y = 30 \text{ mm mrad}$ for the nondispersive plane. Contours of these acceptances calculated with the help of (14.26) are given in Fig. 14.3.

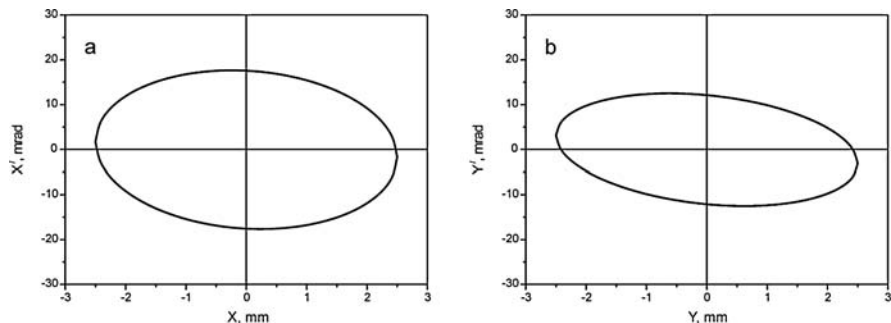


Fig. 14.3. Acceptances of the magnetic analyzer in the new injector leg of the Lund Pelletron accelerator, calculated (a) for the dispersive plane and (b) for the nondispersive plane

14.3 Differential Equations for Beam Envelopes with the Kapchinskiy–Vladimirskiy Density Distribution

Beam envelope calculations performed in a first-order approach are among the most simple and, at the same time, a rather effective way to obtain information about an ion beam with finite emittance. These calculations allow one to find the semiaxis r of the transverse cross section of the beam and the beam divergence r' as functions of the longitudinal coordinate z . Consider a method based on numerical solution of the differential equation for a beam envelope with the Kapchinskiy–Vladimirskiy density distribution [7, 9]. This method is suitable for ion-optical calculations for electrostatic accelerators as the beams for these accelerators have a moderate divergence and relatively low intensity.

Let us assume that the ion-optical channel under consideration includes the following elements: drift sections, axially symmetric electrostatic lenses, sections of the accelerator tube with a uniform field, magnetic and electrostatic quadrupole lenses, dipole analyzing magnets and spherical electrostatic analyzers. To exclude the second derivative of the axial potential $\Phi(z)$ from the envelope equations, we make use of Picht's substitution [14]

$$r_{x,y} = R_{x,y} \Phi^{-0.25} \quad (14.46)$$

which expresses projections of the beam envelope $r_{x,y}$ on the planes XOZ and YOZ by way of the auxiliary variables $R_{x,y}$. If, in (14.46), instead of the potential Φ , one uses the kinetic energy W (expressed in electron volts), the equations for the envelopes of the nonrelativistic ion beam can be written in the following general form [15]:

$$\begin{aligned} R_x'' &= kI/[W(R_x + R_y)] + (W_0\epsilon_x^2)/R_x^3 - (3/16)(W'/W)^2 R_x \pm \omega_x^2 R_x \\ R_y'' &= kI/[W(R_x + R_y)] + (W_0\epsilon_y^2)/R_y^3 - (3/16)(W'/W)^2 R_y \pm \omega_y^2 R_y \end{aligned} \quad (14.47)$$

where I is the beam current in amperes, ϵ_x and ϵ_y denote transverse emittances in mrad, and W_0 is the initial value of the kinetic energy of the ions. The coefficient k is defined by (14.48):

$$k = \frac{Z_i}{2\pi\epsilon_0} \sqrt{\frac{A}{2\eta_0}} \quad (14.48)$$

where Z_i and A stand for the ion charge state and mass number, respectively; $\epsilon_0 = 8.85 \cdot 10^{-12}$ F/m; and $\eta_0 = 0.958 \times 10^8$ C/kg. The coefficients $\omega_{x,y}^2$ describe focusing (–) and defocusing (+) effects of the linear ion-optical elements. For the different ion-optical elements mentioned above, the coefficients $\omega_{x,y}^2$ have the following values and expressions:

- **Drift space:** $\omega_{x,y}^2 = 0$.
- **Axially symmetric electrostatic lens:** $\omega_{x,y}^2 = 0$.
- **Uniform electrostatic field:** $\omega_{x,y}^2 = 0$.
- **Electrostatic quadrupole lens:** $\omega_{x,y}^2 = (Z_i U)/(a^2 W)$, where U is the voltage applied to the lens electrodes in V, and a is the aperture radius of the lens in m.
- **Magnetic quadrupole lens:** $\omega_{x,y}^2 = Z_i G_{x,y}(\eta_0/(2AW))^{0.5}$, where $G_{x,y}$, in T/m, stands for the gradients of the magnetic flux density.
- **Magnetic analyzer:** $\omega_x^2 = (1 - n)/\rho_m^2$ in the dispersive plane, and $\omega_y^2 = n/\rho_m^2$ in the nondispersive plane, where n is a field index and ρ_m is the bending radius in m.
- **Spherical electrostatic analyzer:** $\omega_x^2 = 1/\rho_e^2$ in the dispersive plane, and $\omega_y^2 = 1/\rho_e^2$ in the nondispersive plane, where ρ_e is the bending radius in m.

In the framework of this method, the electrostatic field on node points of the ion-optical axis is determined by the numerical solution of the Dirichlet problem

$$\frac{\partial^2 \Phi}{\partial r^2} + \frac{1}{r} \frac{\partial \Phi}{\partial r} + \frac{\partial^2 \Phi}{\partial z^2} = 0, \quad \Phi_S = U_i \quad (14.49)$$

where U_i is the potential of the i th electrode. The continuous distribution of the axial potential is approximated by a cubic spline.

The need for calculation of a multielectrode axially symmetric electrostatic lens is rather common in studies of the ion-optical system of an electrostatic accelerator. If the potentials of the electrodes attain only two independently variable values, then, having solved the Dirichlet problem for a pair of arbitrarily selected unequal potentials, one can easily determine potentials on the optical axis for any regime of the lens. In the case of more than two independently variable potentials the field calculation becomes complicated, inasmuch as one solution to the boundary problem is now insufficient for all regimes of the lens to be described. In principle it is possible to seek an individual solution to the Dirichlet problem for each of those regimes. However, such an approach to the problem looks rather unpractical from a computational point of view. Another way is to apply the superposition principle to some totality of solutions to the Dirichlet problem. In this case the potential on the optical axis of an n -electrodes lens can be expressed in the following way:

$$\Phi(r, z) = \sum_{i=1}^{n-1} (U_i - U_{i+1}) \Phi_i + U_n \Phi_n \quad (14.50)$$

where $\Phi_1(r, z) - \Phi_n(r, z)$ are solutions to the Dirichlet problem obtained for the linearly independent vectors of the boundary condition $\mathbf{S}_1(1, 0, 0, \dots, 0)$, $\mathbf{S}_2(1, 1, 0, \dots, 0)$, \dots , $\mathbf{S}_n(1, 1, 1, \dots, 1)$; U_1, U_2, \dots, U_n stand for the potentials of the lens electrodes. Some examples of the application of the superposition technique to calculation of multielectrode lenses, as well as estimations of the resulting error in the calculated field, are given in [16].

14.4 Examples of Beam Envelope Calculations

Consider two examples of the application of the method based on solution of the simultaneous differential equations for the beam envelopes, exploiting results obtained at the 3MV Pelletron accelerator in Lund [17].

14.4.1 The Low Energy Part of the Lund Pelletron Accelerator

Figure 14.4 gives examples of beam envelopes calculated for the low-energy part of the accelerator between the ion source and the stripper. The calculations were performed in connection with the development and installation of a new injector [17]. Carbon ion beams with currents of 5 and 10 μA and normalized emittances of 2π mm mrad $(\text{MeV})^{0.5}$ and 4π mm mrad $(\text{MeV})^{0.5}$, respectively, were considered. We assumed that the following voltages were applied to the electrodes of the ion source and the ion source lens (see Fig. 14.5): $U_1 = -40$ kV, $U_2 = -35$ kV, $U_3 = -29$ kV, $U_4 = -35.4$ kV, $U_5 = -20$ kV and $U_6 = 0$ kV. All voltages except U_4 are similar to those found from experience with test running of the ion source. (U_4 in those tests was varied from -35.6 kV to -36.4 kV, depending mainly on the sputtering conditions.) These results illustrate the beam transport through the low-energy part of the accelerator. The ion source lens, in the form in which it has been provided in the design of the injector, allows ions to be focused into a waist on the beam profile monitor. The voltages of the lens electrodes used in the calculations are in agreement with their experimental values. The shape of the beam

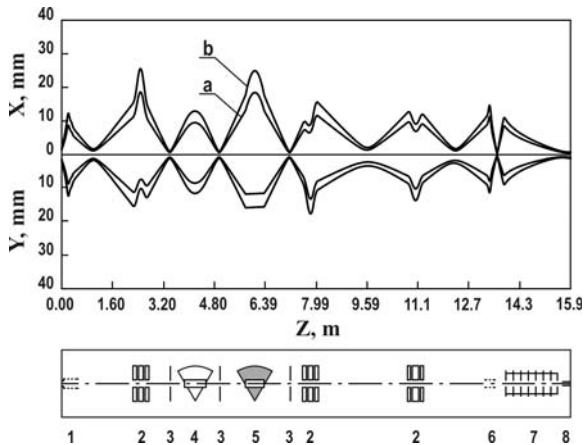


Fig. 14.4. Beam envelopes in the low-energy part of the Lund Pelletron accelerator. Calculations were carried out for a carbon ion beam under the following conditions: (a) $I = 5 \mu\text{A}$, $\epsilon_n = 2\pi$ mm mrad $(\text{MeV})^{0.5}$, (b) $I = 10 \mu\text{A}$, $\epsilon_n = 4\pi$ mm mrad $(\text{MeV})^{0.5}$. Numerals: 1, ion source lens; 2, electrostatic quadrupole triplet; 3, slit device; 4, spherical electrostatic analyzer; 5, magnetic analyzer; 6, einzel lens; 7, accelerator tube; 8, stripper

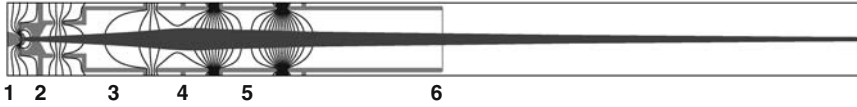


Fig. 14.5. SIMION simulation of C^- beam in the ion source section. Numerals: 1, cathode of the sputtering ion source; 2, spherical ionizer; 3, extracting electrode; 4, focusing electrode; 5, preaccelerating electrode; 6, accelerating electrode

within the electrostatic and magnetic analyzers found from these calculations indicates that the beam emittances are matched to the acceptances of the analyzer section in both transverse planes. In the dispersive plane of the analyzers, the calculated beam occupies approximately half of the aperture of the vacuum chamber. In the nondispersive plane of the magnetic analyzer, the beam transport conditions are somewhat worse. However, the transverse dimension of the beam in this case does not exceed the chamber constraints either. And finally, the ion-optical system of the new injector provides the conditions necessary to match the beam emittance and acceptance of the accelerator tube and to have a beam waist at the stripper position.

14.4.2 Ion Source Lens

To verify the calculation results for the ion source lens obtained by numerical solution of the differential equation for the beam envelopes, these calculations were repeated by use of the SIMION ion-optics simulation program [18]. Result of the SIMION simulation of the carbon ion beam in the part of the ion-optical system between the sputtered sample and the beam profile monitor, performed for the same electrode voltages as in the previous example, are given in Fig. 14.5.

The beam envelopes found from numerical solution of the differential equations (14.47) and from the SIMION simulation are given in Fig. 14.6. The calculations were carried out for two pairs of values of the beam current and emittance, namely $I = 5 \mu\text{A}$, $\epsilon_n = 2\pi \text{ mm mrad (MeV)}^{0.5}$ (Fig. 14.6, part a) and $I = 10 \mu\text{A}$, $\epsilon_n = 4\pi \text{ mm mrad (MeV)}^{0.5}$ (Fig. 14.6, part b). In both cases, the results obtained by these two different methods are in good agreement. Some differences between the beam geometries are observed. The plane of the beam waist calculated by SIMION has a small shift toward the lens. It can be explained by the influence of geometrical aberrations, which are not taken into account in the framework of the paraxial approximation used in the beam envelope method. The fact that the differences are reduced with decreasing emittance value (this value defines the highest possible angle of the ion trajectory in the beam) indicates the consistency of this assumption.

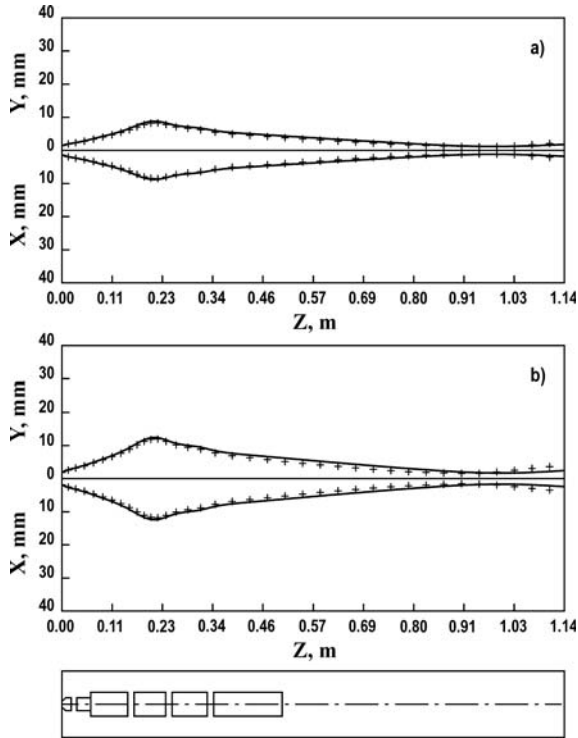


Fig. 14.6. C^- beam envelopes in the lens of the spherical-ionizer sputtering ion source, found by different calculation techniques (+++ SIMION simulation, — beam envelope method) for two values of the emittance: (a) 2π mm mrad $(\text{MeV})^{0.5}$ and (b) 4π mm mrad $(\text{MeV})^{0.5}$

References

1. H. Wollnik: *Optics of Charged Particles* (Academic Press, New York, 1987)
2. M. Szilgyi: *Electron and Ion Optics* (Plenum, New York, 1988)
3. P.W. Hawkes, E. Kasper: *Principles of Electron Optics* (Academic Press, New York, 1989)
4. M. Elkind: *Rev. Sci. Instr. A* **24**:2, 129 (1953)
5. J.D. Larson: *Nucl. Instr. Meth. A* **244**, 192 (1986)
6. K.L. Brown: *Nucl. Instr. Meth.* **187**, 51 (1981)
7. V.A. Tepljakov: *Instr. Exp. Tech.* **6**, 13 (1968) (in Russian)
8. J.D. Lawson: *The Physics of Charged-Particle Beams* (Clarendon Press, Oxford, 1977)
9. I.M. Kapchinskiy: *Particle Dynamics in Linear Resonance Accelerators* (Atomizdat, Moscow, 1966) (in Russian)
10. E.V. Shpak: *Nucl. Instr. Meth.* **213**, 171 (1983)
11. R. Hellborg, K. Håkansson, G. Skog: *Nucl. Instr. Meth. A* **287**, 161 (1990)
12. J.D. Larson, C.M. Jones: *Nucl. Instr. Meth.* **140**, 489 (1977)

13. R. Hellborg, M. Faarinen, C.E. Magnusson, S. Bazhal, V. Romanov: Nucl. Instr. Meth. A **465**, 297 (2001)
14. A.P. Banford: *The Transport of Charged Particle Beams* (Spon, London, 1966)
15. S. Bazhal, M. Faarinen, R. Hellborg, C.E. Magnusson, V. Romanov: Proceedings of the 13th International Conference on Electrostatic Accelerators, 25–28 May 1999, Obninsk, Russia, p. 160
16. S.V. Bazhal and V.A. Romanov: Proceedings of the 12th International Conference on Electrostatic Accelerators, 25–28 Nov. 1997, Obninsk, Russia, p. 229 (in Russian)
17. R. Hellborg, S. Bazhal, M. Faarinen, K. Håkansson, C.E. Magnusson, P. Persson, G. Skog, K. Stenström: Pramana – J. of Physics **59**:5, 1 (2002)
18. D.A. Dahl: SIMION 3D, Version 7.0, User's manual, Idaho National Engineering and Environmental Laboratory, INEEL-95/0403 (2000)